Predictive Duty Cycle Control of Three-Phase Active-Front-End Rectifiers

Zhanfeng Song, *Member, IEEE*, Yanjun Tian, *Student Member, IEEE*, Wei Chen, *Member, IEEE*, Zhibin Zou, and Zhe Chen, *Senior Member, IEEE*

***Abstract*—This paper proposed an online optimizing duty cycle control approach for three-phase active-front-end rectifiers, aiming to obtain the optimal control actions under different operating conditions. Similar to finite-control set model predictive control strategy, a cost function previously constructed based on the desired control performance is adopted here, which is essential for the solving process of the optimizing problem. On the other hand, differently, with respect to the proposed strategy, duty cycle signals are optimized, instead of possible switching states. The determination of optimal duty cycles is made by predicting the effect of duty cycles on instantaneous current variations and minimizing the cost function. Due to the adoption of behavior prediction, the proposed controller inherits the excellent dynamic characteristics of predictive controllers. Moreover, the application of optimal duty cycles determined by cost function minimization automatically ensures optimum operations of converters within each sampling period. Improved transient and steady-state features of the proposed strategy are confirmed by experimental validations and in-depth comparisons with linear controllers, deadbeat predictive controllers, and finite-control set model predictive control strategies.**

***Index Terms*—Predictive control, cost function minimization, three-phase active-front-end rectifier.**

I. Introduction

As one of the most popular converter topologies used in industrial applications, three-phase active-front-end rectifiers have been in continuous development recently. Main features of three-phase active-front-end rectifiers include bidirectional power flow, nearly sinusoidal input currents, unity power factor, and flexible regulation of dc-link voltage. The control of three-phase active-front-end rectifiers has been an active research topic in the area of power conversion.

With the aim of flexible regulation of powers and currents, different kinds of control techniques have been developed. Linear control methods, like PI controllers implemented together with pulse width modulation (PWM), are most widely used. For the design of these controllers, the converters are normally modeled as a linear system, and a transfer function of converters should be obtained, based on which control parameters are tuned accordingly. Excellent steady-state performances can be observed when this type of controllers is adopted. Besides, a fixed switching frequency can also be expected due to the adoption of modulation stage. However, due to the bandwidth limitation of PI regulators, significant errors normally appear during the tracking process of the high-order components in the current reference. For the current control of three-phase active-front-end rectifiers, this item reflects in unsatisfactory dynamic transient responses. In other words, high dynamic transient responses cannot be ensured in this case, which is quite important for the inner loop current control of converters.

During the past several years, different control techniques have also been proposed, with the aim of improving system performances. Model predictive control emerges as a useful tool for the control of power conversion with great potential [1]–[3]. One typical application form of model predictive control is deadbeat predictive (DBP) control, which has been widely used in different applications. This type of controllers attempts to eliminate the control error within one switching period. In other words, DBP controller adjusts the current so that it tracks its reference value at the end of the next switching period [4]. The application process of DBP controllers includes two separate steps. First, the required output voltage to be produced by the converters is calculated based on the current error and model information. Second, switching signals are then obtained on the basis of modulation [5]. Belonging to the family of model predictive control strategies, DBP controllers possess theoretically a high bandwidth, and therefore, highly dynamic transient behaviors can be successfully achieved [6]. However, as mentioned previously, the required output voltage of the converter is directly determined based on current errors and model information, without the modulation process and switching actions taken into account. During the experimental studies, it is found that this might result in unsatisfactory reference-tracking performances under certain situations, which can be clearly seen in the experimental results shown in the following sections.

As one of the most popular predictive controllers widely used recently, finite-control set model predictive control (FCS-MPC) is now experiencing an explosive evolution [7], [8]. Different from DBP controllers, FCS-MPC regards the current control problem of converters as an online optimization process, which takes discrete switching actions, reference tracking, and control constraints into consideration. Within each sampling period, converter behaviors are predicted for all the finite-switching states on the basis of system model information, converter parameters and measurements. A predefined cost function dependent on the desired behaviors is evaluated for each prediction.

Manuscript received August 23, 2014; revised November 21, 2014; accepted January 8, 2015. Date of publication February 2, 2015; date of current version September 21, 2015. This work was supported by the National Natural Science Foundation of China under Grant 51107084 and Grant 51477113. Recommended for publication by Associate Editor Y. Xing.

Z. Song and W. Chen are with the School of Electrical Engineering and Automation, Tianjin University, Tianjin 300072, China (e-mail: zfsong@tju.edu.cn; chen_wei@tju.edu.cn).

Y. Tian and Z. Chen are with the Department of Energy Technology, Aalborg University, Aalborg 9100, Denmark (e-mail: yti@et.aau.dk; zch@et.aau.dk).

Z. Zou is with State Grid Jiangxi Electric Power Company, Nanchang 330006, China (e-mail: bingojxzzb@163.com).

Color versions of one or more of the figures in this paper are available online at http://ieeexplore.ieee.org.

Digital Object Identifier 10.1109/TPEL.2015.2398872

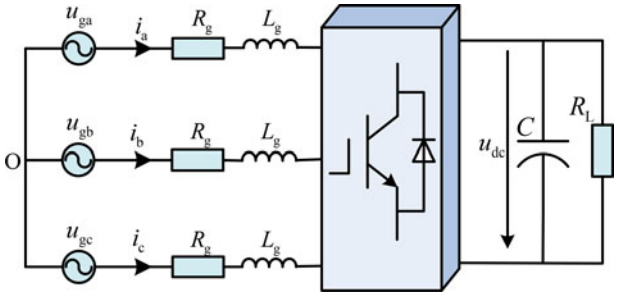

Fig. 1. Typical structure of a three-phase active-front-end rectifier.

The switching state which results in the minimum cost function is selected and finally applied [9]–[12]. The major advantage of this control strategy lies in its online optimization characteristics. The optimal control action for the next sampling period can be easily obtained based on cost function minimization [13]–[19]. However, there are some practical challenges for finite-control set model predictive controllers to be tackled, including the model parameter dependence [20]–[22], steady-state performances [23]–[25], and the variable switching frequency [26]–[28].

This paper seeks to propose an online optimizing control strategy for three-phase active-front-end rectifiers, aiming to obtain the optimal control actions under different operating conditions. Similar to FCS-MPC, a cost function previously constructed based on the desired control performance is adopted here, which is essential for the solving process of the optimizing problem. However, differently, with respect to the proposed strategy, duty cycle signals are to be optimized, instead of possible switching states. The determination of optimal duty cycles is made by predicting the effect of duty cycles on instantaneous current variations and minimizing the cost function. Therefore, the application of optimal duty cycles automatically ensures optimum operations of converters within each sampling period. This paper is organized as follows. The operating principle of the proposed strategy is presented in Section II, as well as the instantaneous current behaviors of three-phase active-front-end rectifiers. In Section III, the test bench equipped with a 11-kW-Danfoss converter is briefly depicted. Corresponding experimental validations and detailed analysis are both provided. Section IV presents in-depth comparisons with traditional linear controllers, DBP controllers, and FCS-MPC strategies, during steady-state, transient, grid filter parameter variations, and robustness against grid disturbances. Finally, conclusions are drawn in Section V.

II. Predictive Duty Cycle Control Based on Cost Function Minimization

The typical structure of a three-phase active-front-end rectifier is shown in Fig. 1, where u_g and $u_{\rm dc}$ represent the grid phase voltage and the dc-link voltage, respectively. *i* denotes the phase current. L_g is the inductance of the grid filter and R_g represents its equivalent resistance. *C* and R_L denote the dc-link capacitor and the load resistance, respectively.

Its mathematical model in stationary α-β reference frame can be written as

$$u_{g\alpha} = L_g \frac{{\rm d}i_\alpha}{{\rm d}t} + R_g i_\alpha + u_{c\alpha} \tag{1}$$

$$u_{g\beta} = L_g \frac{{\rm d}i_\beta}{{\rm d}t} + R_g i_\beta + u_{c\beta} \tag{2}$$

where $u_{g\alpha}$ and $u_{g\beta}$ are the α- and β-axes components of grid voltage vector. i_α and i_β are the α- and β-axes components of phase current vector. $u_{c\alpha}$ and $u_{c\beta}$ are the output voltage components of the active-front-end rectifier.

Based on the previous equations, the voltage equations in synchronous *d-q* reference frame can be obtained as follows:

$$u_{gd} = L_g \frac{{\rm d}i_d}{{\rm d}t} + R_g i_d - \omega_g L_g i_q + u_{cd} \tag{3}$$

$$u_{gq} = L_g \frac{{\rm d}i_q}{{\rm d}t} + R_g i_q + \omega_g L_g i_d + u_{cq} \tag{4}$$

where subscripts *d* and *q* represent *d*- and *q*-axes components, respectively.

After rearrangement, (3) and (4) can be expressed as

$$\frac{{\rm d}i_d}{{\rm d}t} = \frac{1}{L_g}(-R_g i_d + \omega_g L_g i_q - u_{cd} + u_{gd}) \tag{5}$$

$$\frac{{\rm d}i_q}{{\rm d}t} = \frac{1}{L_g}(-R_g i_q - \omega_g L_g i_d - u_{cq} + u_{gq}). \tag{6}$$

Normally, two adjacent voltage vectors in the vector span are selected during the calculation process of the proposed predictive duty cycle control (PDC). These two adjacent voltage vectors can be selected at random without influencing controller performances. In this paper, $\boldsymbol{V}_1$ and $\boldsymbol{V}_2$ are selected as an example. Obviously, the corresponding numerical relationship among phase duty cycles d_a, d_b, and d_c is $d_a > d_b > d_c$ under this situation. The application time of $\boldsymbol{V}_1$ during one sampling period T_s is equal to $(d_a - d_b)T_s = (1 - d_b - d_c)T_s$. In a similar way, the application time of $\boldsymbol{V}_2$ during one sampling period T_s is $(d_b - d_c)T_s$. The application time of zero voltage vectors is thus $T_s - (1 - d_b - d_c)T_s - (d_b - d_c)T_s = 2d_c T_s$.

Based on (5) and (6), the derivatives of *d*- and *q*-axes currents generated by the application of voltage vectors $\boldsymbol{V}_1$ and $\boldsymbol{V}_2$ can be, respectively, obtained as

$$\delta_{d,1} = \frac{{\rm d}i_d}{{\rm d}t}\Big|_{V=V_1}, \quad \delta_{d,2} = \frac{{\rm d}i_d}{{\rm d}t}\Big|_{V=V_2} \tag{7}$$

$$\delta_{q,1} = \frac{{\rm d}i_q}{{\rm d}t}\Big|_{V=V_1}, \quad \delta_{q,2} = \frac{{\rm d}i_q}{{\rm d}t}\Big|_{V=V_2}. \tag{8}$$

For the chosen example, $\boldsymbol{V}_1$ and $\boldsymbol{V}_2$ are adopted during the calculation process of the proposed algorithm. In this case, *d*- and *q*-axes current increments under the voltage vectors $\boldsymbol{V}_1$, $\boldsymbol{V}_2$ with the duty cycles d_a, d_b, and d_c can be computed as

$$e_{d,1} = \delta_{d,1}\left[(d_a - d_b)T_s\right] = \delta_{d,1}\left[(1 - d_b - d_c)T_s\right] \tag{9}$$

$$e_{d,2} = \delta_{d,2}\left[(d_b - d_c)T_s\right] \tag{10}$$

$$e_{d,0} = 2\delta_{d,0} d_c T_s \tag{11}$$

$$e_{q,1} = \delta_{q,1}\left[(d_a - d_b)T_s\right] = \delta_{q,1}\left[(1 - d_b - d_c)T_s\right] \tag{12}$$

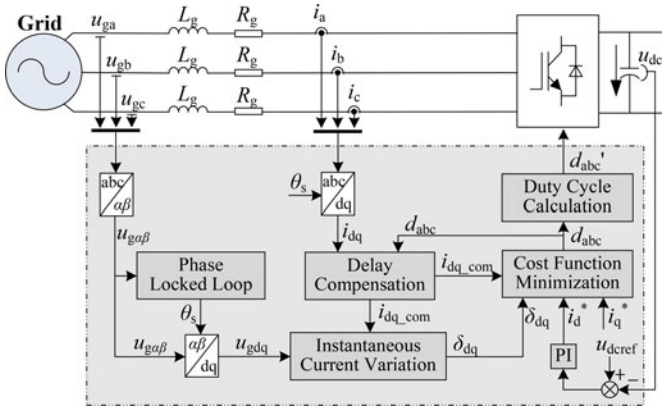

Fig. 2. Control structure of the proposed PDC.

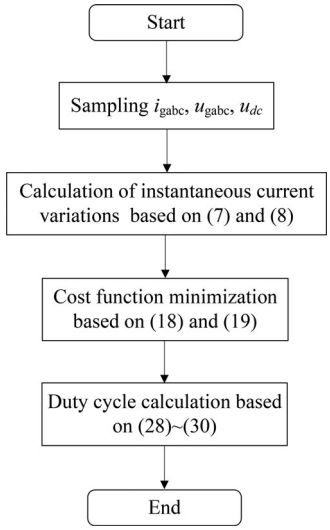

Fig. 3. Flowchart of the proposed PDC.

$$e_{q,2} = \delta_{q,2}\left[(d_b - d_c)T_s\right] \tag{13}$$

$$e_{q,0} = 2\delta_{q,0} d_c T_s. \tag{14}$$

Current control errors can be expressed as

$$\Delta i_d = i_d^* - i_d - e_{d,0} - e_{d,1} - e_{d,2} \tag{15}$$

$$\Delta i_q = i_q^* - i_q - e_{q,0} - e_{q,1} - e_{q,2} \tag{16}$$

where i_d^* and i_q^* represent the reference values of the d- and q-axes currents, respectively.

It is expected that the currents evolve from their initial values toward the reference values during control period T_s. As a consequence, the cost function should be constructed as follows:

$$g = \Delta i_d^2 + \Delta i_q^2. \tag{17}$$

The optimum duty cycles satisfies the following expression:

$$\frac{\partial g}{\partial d_a} = \frac{\partial(\Delta i_d^2 + \Delta i_q^2)}{\partial d_a} = 0 \tag{18}$$

$$\frac{\partial g}{\partial d_b} = \frac{\partial(\Delta i_d^2 + \Delta i_q^2)}{\partial d_b} = 0. \tag{19}$$

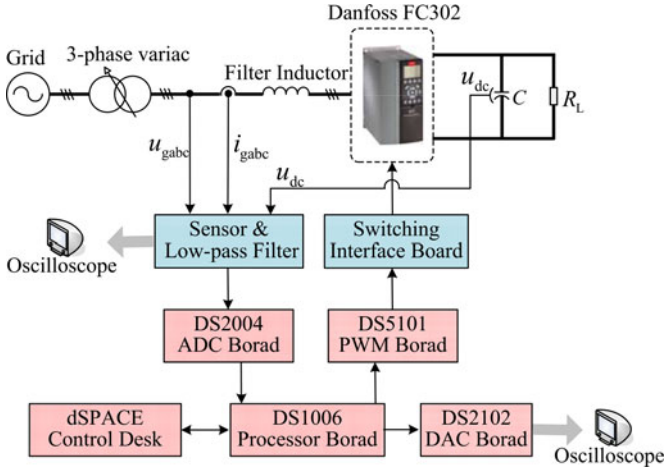

Fig. 4. Configuration of the experimental platform.

TABLE I
PARAMETERS OF THE EXPERIMENTAL PLATFORM

Parameters		Value
Rated power	P	1.8 kW
Output voltage of the variac	u_g	245 V
Grid frequency	f	50 Hz
Equivalent resistance	R_g	0.1 Ω
Filter inductance	L_g	7.8 mH
DC-link capacitor	C	950 μF
Switching frequency	f_s	10 kHz
DC-link voltage	u_{dc}	420 V

Based on (9)–(16), (18), and (19), the duty cycles can thus be obtained as

$$\begin{aligned} d_a = {} & \frac{1}{2mT_s}[(i_d^* - i_d)(\delta_{q,2} - \delta_{q,1}) + (i_q^* - i_q)(\delta_{d,1} - \delta_{d,2}) \\ & + 2T_s\delta_{q,0}(\delta_{d,2} - \delta_{d,1}) - 2T_s\delta_{d,0}(\delta_{q,2} - \delta_{q,1}) \\ & + T_s\delta_{d,1}\delta_{q,2} - T_s\delta_{d,2}\delta_{q,1})] \end{aligned} \tag{20}$$

$$\begin{aligned} d_b = {} & \frac{1}{2mT_s}[(i_d^* - i_d)(2\delta_{q,0} - \delta_{q,1} - \delta_{q,2}) \\ & + (i_q^* - i_q)(\delta_{d,1} + \delta_{d,2} - 2\delta_{d,0}) \\ & + T_s\delta_{q,1}(2\delta_{d,0} - \delta_{d,2}) + T_s\delta_{d,1}(\delta_{q,2} - 2\delta_{q,0})] \end{aligned} \tag{21}$$

$$d_c = 1 - d_a \tag{22}$$

where

$$m = (\delta_{q,2} - \delta_{q,0})\delta_{d,1} - (\delta_{q,1} - \delta_{q,0})\delta_{d,2} - (\delta_{q,2} - \delta_{q,1})\delta_{d,0}. \tag{23}$$

It is well known that, resulting from the calculation and sampling process, control delay exists during the implementation of the control algorithm [29]. Hence, control actions cannot be performed instantly in real applications. Normally, predictive controllers suffer from the control delay. In order to eliminate performance deteriorations caused by the control delay, the following compensation measures should be adopted here. The

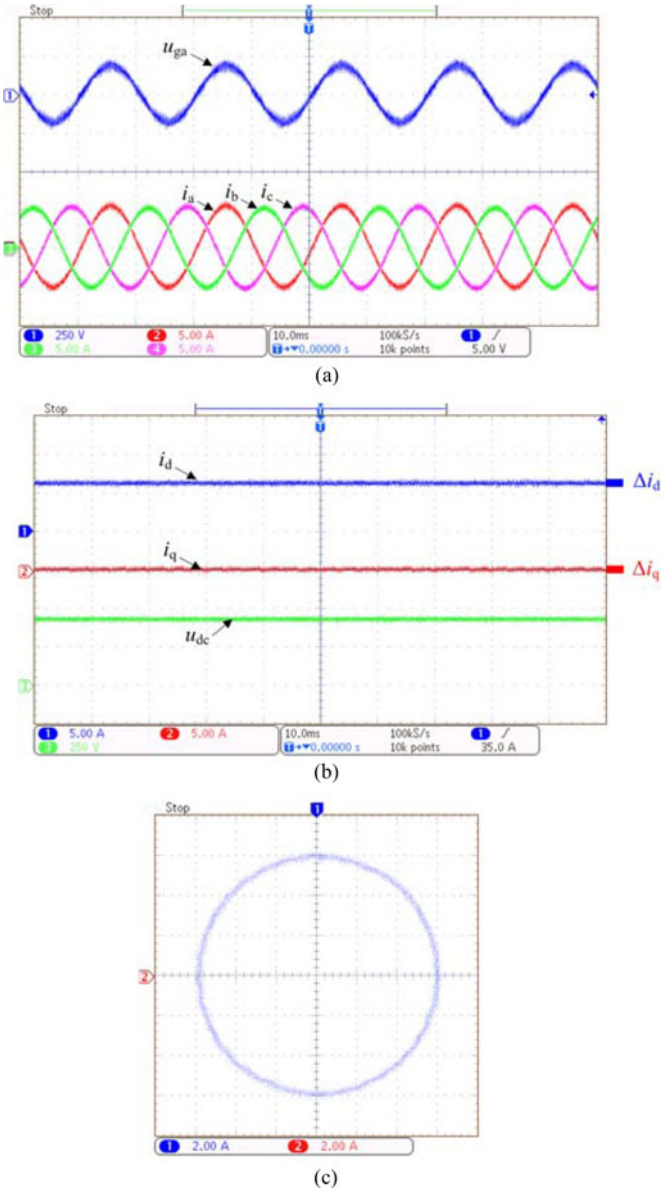

Fig. 5. System behaviors in steady-state operation when PDC is adopted. (a) Grid voltage and phase currents. (b) d-q currents and dc voltage. (c) Phase currents in the α-β reference frame.

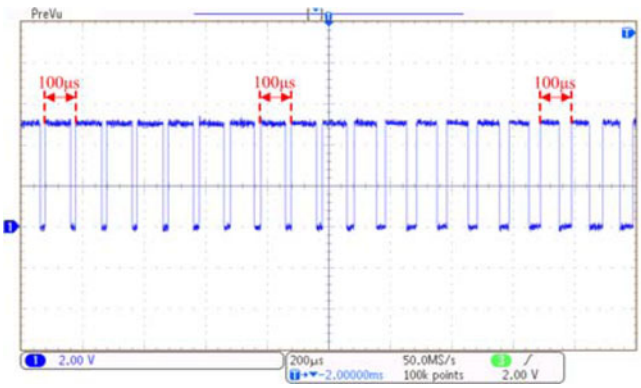

Fig. 6. PWM signals when PDC is adopted.

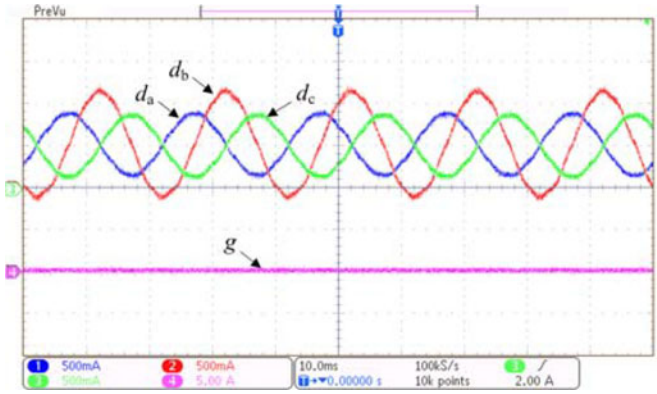

Fig. 7. Cost function g and three-phase duty cycles obtained based on cost function minimization with $\boldsymbol{V}_1$ and $\boldsymbol{V}_2$ adopted during the performing process of the control algorithm.

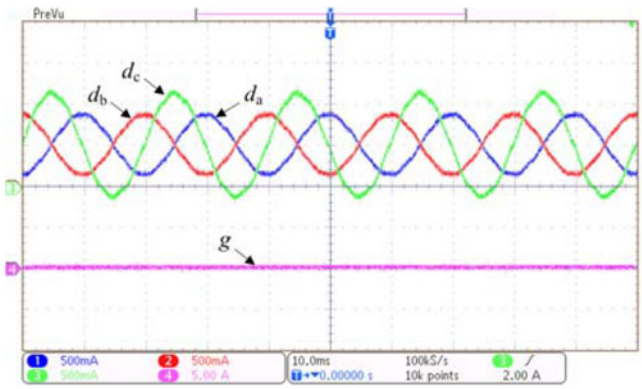

Fig. 8. Cost function g and three-phase duty cycles obtained based on cost function minimization with $\boldsymbol{V}_3$ and $\boldsymbol{V}_4$ adopted during the performing process of the control algorithm.

compensation current components can be calculated as

$$\Delta i_{d\_\mathrm{com}} = d_c\delta_{d,0} + (d_a - d_b)\delta_{d,1} + (d_b - d_c)\delta_{d,2} \quad (24)$$

$$\Delta i_{q\_\mathrm{com}} = d_c\delta_{q,0} + (d_a - d_b)\delta_{q,1} + (d_b - d_c)\delta_{q,2}. \quad (25)$$

The current value after delay compensation should be computed as

$$i_{d\_\mathrm{com}} = i_d + \Delta i_{d\_\mathrm{com}} \quad (26)$$

$$i_{q\_\mathrm{com}} = i_q + \Delta i_{q\_\mathrm{com}}. \quad (27)$$

According to common sense, the value of switch duty cycles can only lie in the closed interval [0, 1]. However, when computed based on (20)–(22), the value of switch duty might be larger than one, or smaller than zero. Obviously, this is unacceptable in the implementation of control algorithms, and, therefore, the calculated duty cycles cannot be directly transferred to the converters.

Actually, current variations are determined by the applications of voltage vectors. If the application times of nonzero voltage vectors are kept unchanged, the current tracking performances will surely be achieved. And as mentioned previously, the application times of nonzero voltage vectors are proportional

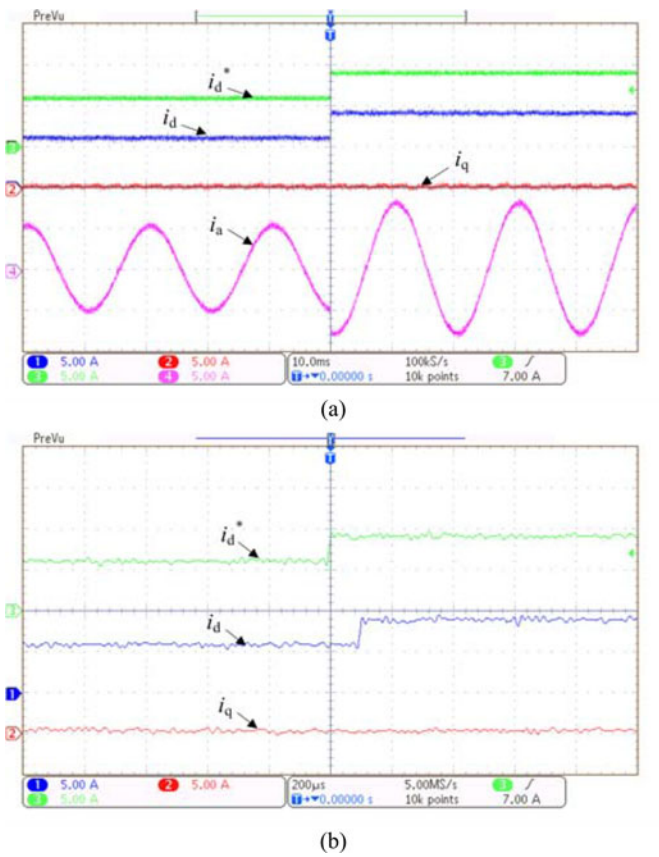

Fig. 9. Instantaneous current behaviors with a step change of d-axis reference current when PDC is adopted. (a) Current behaviors. (b) Zoom window of current behaviors.

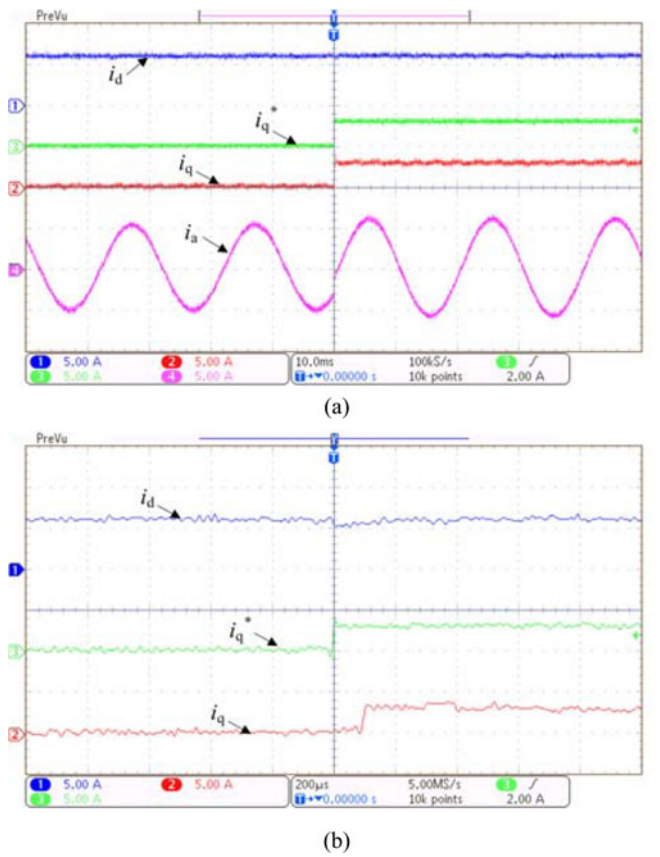

Fig. 10. Instantaneous current behaviors with a step change of q-axis reference current when PDC is adopted. (a) Current behaviors. (b) Zoom window of current behaviors.

to $d_a - d_b$ and $d_b - d_c$, respectively. This indicates that adding or reducing the same quantity to the values of all duty cycles will not affect the application times of nonzero voltage vectors. As a consequence, the desired reasonable values of duty cycles can be calculated as

$$d'_a = d_a - \min(d_a, d_b, d_c) + \frac{1 - \max(d_a, d_b, d_c) + \min(d_a, d_b, d_c)}{2} \quad (28)$$

$$d'_b = d_b - \min(d_a, d_b, d_c) + \frac{1 - \max(d_a, d_b, d_c) + \min(d_a, d_b, d_c)}{2} \quad (29)$$

$$d'_c = d_c - \min(d_a, d_b, d_c) + \frac{1 - \max(d_a, d_b, d_c) + \min(d_a, d_b, d_c)}{2}. \quad (30)$$

These calculated duty cycles d'_a, d'_b, and d'_c are then transferred to the converter and finally applied in the next control period. To further show how the proposed algorithm works, the corresponding control structure is shown in Fig. 2, and its flowchart is demonstrated in Fig. 3. As demonstrated by these figures, a cost function should be constructed based on desired control performances and current tracking errors. The effects of duty cycles on current behaviors are then predicted on the basis of system instantaneous characteristics. Finally, optimization of duty cycle signals is realized by means of cost function minimization. The control structure of the whole system can be summarized as follows. d-Axis current reference is first obtained with the assistance of outer dc voltage loop, while q-axis current reference is obtained based on system requirements. Current regulation is then realized by duty cycle prediction and cost function minimization. It is worth mentioning that this

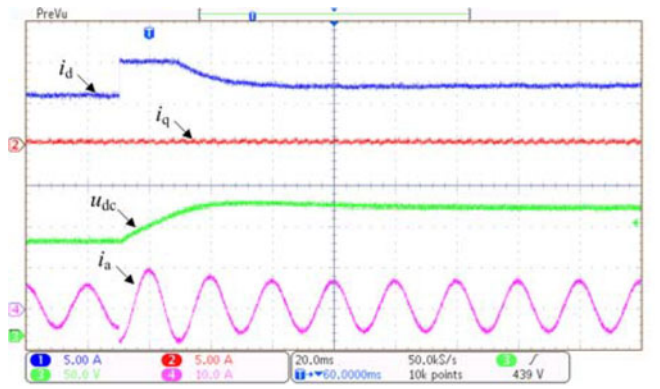

Fig. 11. Instantaneous behaviors with a step change of dc reference voltage when PDC is adopted (offset voltage of u_{dc}: 300 V).

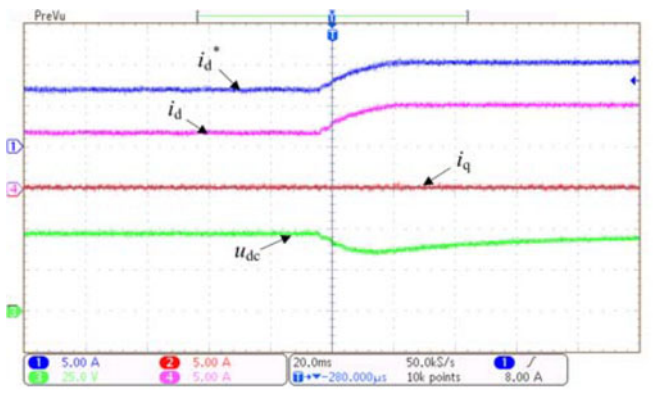

Fig. 12. System transient responses to external load disturbances when PDC is adopted.

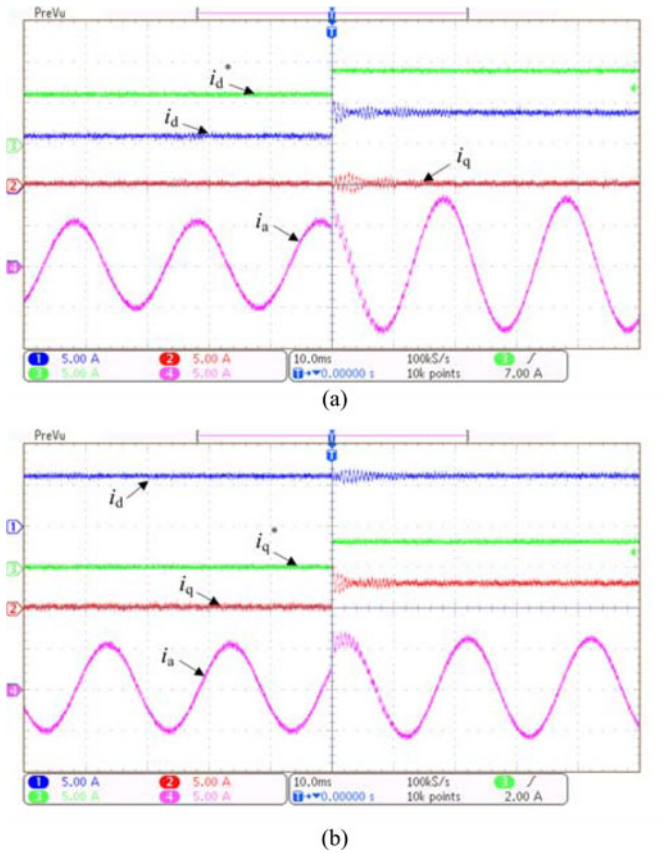

Fig. 13. Instantaneous current behaviors without delay compensation. (a) Current behaviors with a step change of d-axis reference current. (b) Current behaviors with a step change of q-axis reference current.

proposed duty cycle control method is independent of vector selection. This will be further verified by the following experimental results.

III. Performance Investigation

In order to experimentally evaluate the steady-state and transient performances of the proposed PDC, a laboratory-scale experimental platform was built up, whose main components are presented in Fig. 4. A three-phase variac and a filter inductor are used to connect the experimental platform and the ac supply. A commercial Danfoss FC302 converter based on insulated-gate bipolar transistors is used as an active-front-end rectifier. A dSPACE DS1006 board is adopted to carry out the control algorithms, as well as communicating with the dSPACE control desk. Besides, the platform is equipped with some accessory interface boards, including DS 2004 ADC board, DS5101 PWM board, and DS2102 DAC board, for the signal sampling, PWM signal generating, and digital-to-analog transforming. Moreover, LEM sensors and Butterworth low-pass filters are both used for the sampling of currents and voltages. The experimental platform parameters are presented in Table I. Besides, DPO3014 Oscilloscope from Tektronix and associated devices are used to capture the experimental waveforms. It should be noted that even though dSPACE DS1006 board is used here to carry out the proposed control algorithm demonstrated in Fig. 3, the computation capability of commercial DSP TMS320F28335 is sufficient for running the proposed PDC control strategy. And the corresponding running time is around 70 μs.

A. Steady-State Performances

In order to illustrate the feasibility of the proposed strategy, experimental studies were initially carried out regarding the steady-state performances. Fig. 5 shows the experimentally obtained waveforms of the grid voltage and three-phase currents, with the reference values of d- and q-axes current being 6 and 0 A, respectively. In addition, the dc voltage and phase currents in the α-β reference frame are also presented, as well as d- and q-axes currents. It is clearly shown by these experimental results that the proposed strategy can achieve proper regulation of d- and q-axes currents, which are both maintained constant during the operation of the rectifier. As can be seen in Fig. 5(b), the fluctuation ranges of d- and q-axes currents are both quite limited, indicating the excellent capability of current regulation presented by the proposed PDC. Besides, as expected, three phase currents are balanced and sinusoidal. And the phase current is kept in phase with the corresponding grid voltage due to the fact that the rectifier is operating in the unity power factor mode. Furthermore, it is clearly visible in Fig. 5(c) that the profile of phase currents in the α-β reference frame is an ideal circle, and the trajectory of phase currents lies in a relatively narrow band, confirming the distinguished steady-state performances of the proposed PDC strategy.

To further evaluate system performances with regard to the switching frequency, experimental behaviors of PWM signals sent out by the PDC are shown in Fig. 6. This result was obtained under the same operating conditions with those of Fig. 5. As can be observed in this illustrative waveform, with the assistance of duty cycle regulation, the switching frequency is surely kept constant at all times when the proposed PDC algorithm is adopted, which is a favorable characteristic for the power conversion and the design of grid filters.

As argued previously in Section III, even though the analysis and calculation for the chosen example are based on the adoption of $\boldsymbol{V}_1$ and $\boldsymbol{V}_2$ as active voltage vectors, control performances

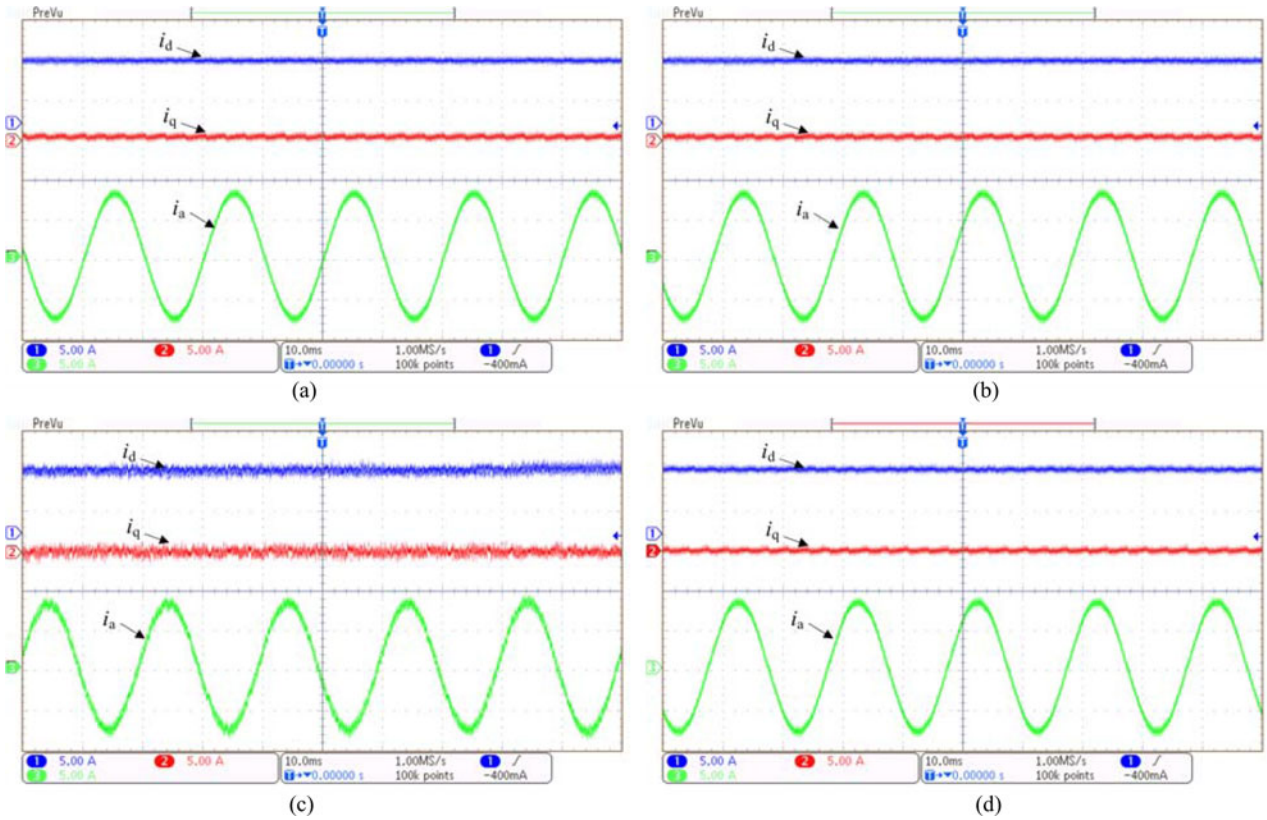

Fig. 14. Experimental results using four different control strategies during steady-state operation. (a) Conventional DBP. (b) Proposed PDC. (c) FCS-MPC. (d) Classic LC.

are actually independent of the selection of voltage vectors. In order to validate this remarkable conclusion, experiments have been conducted accordingly. Fig. 7 demonstrates the value of cost function g and three-phase duty cycles obtained based on cost function minimization with $\boldsymbol{V}_1$ and $\boldsymbol{V}_2$ adopted during the performing process of the control algorithm, while the waveform when $\boldsymbol{V}_3$ and $\boldsymbol{V}_4$ are used is shown in Fig. 8. These results have been obtained under the same operating conditions with that of Fig. 5. It is obvious that selection of different voltage vectors leads to different waveforms of duty cycles. However, as can be clearly appreciated by comparing the waveforms of the cost function g in these two figures, different combination of adjacent voltage vectors results in the same behaviors, without influencing the current-tracking capability and steady-state performances of the control algorithm.

B. Transient Responses

The transient response is an important issue in the operating process of converters, particularly in power conversion of grid-connected converters. With the aim of investigating the transient responses of PDC, a step change between 6 and 9 A is introduced to the d-axis reference current, while the q-axis reference current is constant and maintained zero in this experiment. Instantaneous d- and q-axes current behaviors are shown in Fig. 9(a), as well as the waveform of the phase current. Besides, the zoom window of these transient responses is also provided for clarity. As can be clearly seen in these figures, the step-changed reference current can be quickly followed by the PDC algorithm. It can be measured from Fig. 9(b) that the response time of d-axis current steps from 6 to 9 A is around 100 μs. This indicates that, due to the adoption of behavior prediction and cost function minimization, the proposed PDC can achieve highly dynamic performance and inherit the excellent transient characteristics of predictive controllers. Meanwhile, as shown in Fig. 9, zero steady-state tracking errors can be achieved immediately after the transient process. Furthermore, as can be seen from Fig. 9(a) and 9(b), no significant variations are detected with respect to the q-axis current. This indicates that the proposed PDC strategy can achieve excellent decoupling regulation between d- and q-axes currents at all times, as can be clearly appreciated even during the step transition.

To further illustrate and validate the transient performances of the proposed PDC strategy, similar transient tests were also conducted under the condition of step change in the q-axis reference current. The corresponding step responses of the rectifier and the zoom window are shown in Fig. 10, where the reference of q-axis current steps from 0 to 2 A and the d-axis current remains 6 A. Similar to the situation shown in Fig. 9, it is clearly visible in Fig. 10 that excellent transient performances and proper regulation of q-axis current can be achieved when the proposed PDC strategy is adopted. The q-axis current is rapidly changed in order to follow the new reference signal, with the transient process finished within 100 μs.

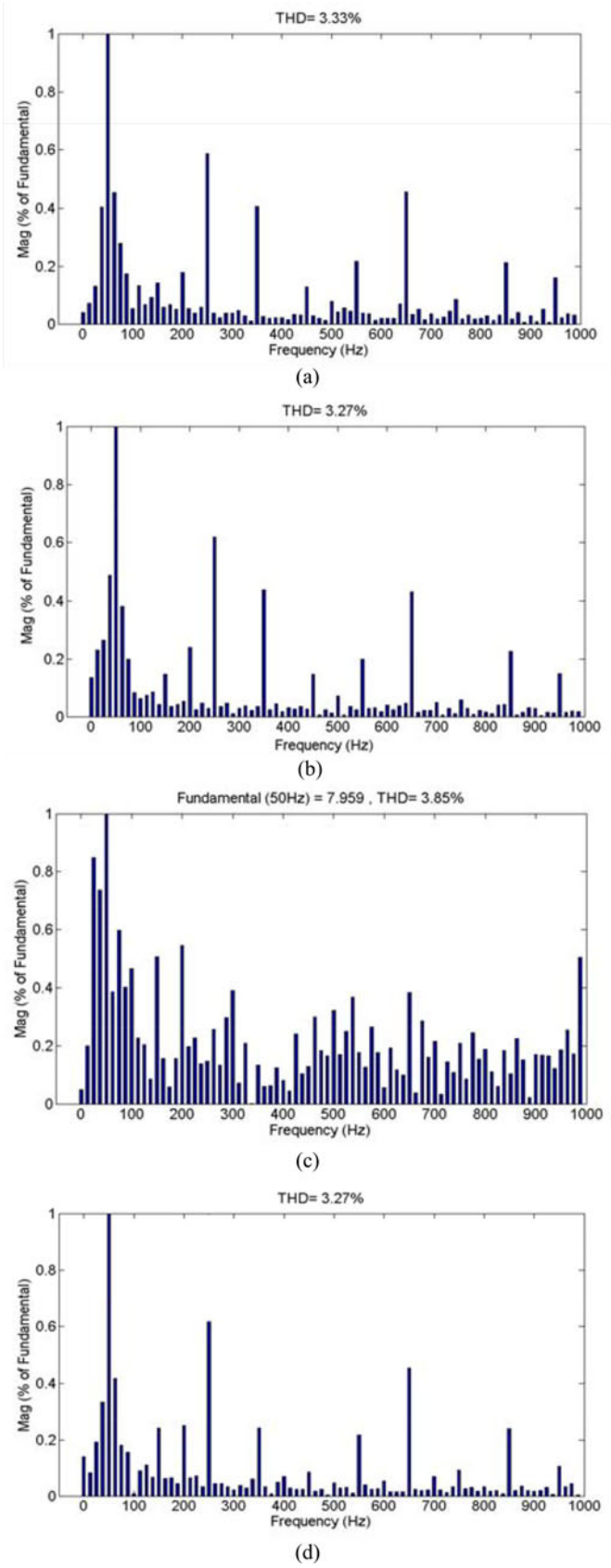

Fig. 15. THD results using four different control strategies during steady-state operation. (a) Conventional DBP. (b) Proposed PDC. (c) FCS-MPC. (d) Classic LC.

Further tests were conducted on the transient responses of the rectifier when the reference dc voltage is step changed from 420 to 470 V. The *d*-axis reference current is obtained from the outer loop voltage controller, while the *q*-axis reference current remains 0 A for unity power factor operation. The corresponding experimental waveforms are shown in Fig. 11, where the offset voltage of $u_{\rm dc}$ is set to 300 V for clarity. When there is a step change in the reference signal of the dc voltage, the *d*-axis reference current rises accordingly due to the voltage errors of the outer control loop.

It is worth noting that, for the chosen example, the current limit is 10 A. Hence, the *d*-axis reference current instantaneously reaches the upper limit in this case, as can be seen in Fig. 11. Due to the excellent dynamic responses of the proposed current control method, the *d*-axis current rises rapidly, resulting in the increase of the dc voltage and the decrease of voltage error. Under this situation, the *d*-axis current decreases accordingly, leading to the amplitude change of phase currents. Note that the *q*-axis current is hardly affected at all by the transient process. Neither the step rise nor the decrease of *d*-axis current has significant impact on the behavior of *q*-axis current. This further illustrates the excellent decoupling regulation performances of PDC.

For further illustration of the effectiveness of PDC, transient tests were also conducted by introducing disturbances to the rectifier, in which the resistance load of the dc link was changed from 126 to 84 Ω. Fig. 12 demonstrates system instantaneous behaviors under this situation. For clarity and better understanding, the *d*-axis reference current generated by the dc voltage control loop is also provided. A transient in the dc voltage during the disturbance response can be clearly observed. The dc voltage drops due to the disturbances of the load resistance, resulting in the increase of the *d*-axis reference current. Obviously, with the actions of the PDC current control strategy, the *d*-axis current can properly track the reference trajectory, as demonstrated in Fig. 12. With the increase of the *d*-axis current, the dc voltage returns to normal accordingly. It should be noted that the *q*-axis current remains constant in this transient process, confirming the excellent decoupling regulation of currents performed by the developed PDC.

C. Effect of Delay Compensation

As mentioned in previous sections, the calculation and sampling process will introduce control delay, which might influence system behaviors if no compensation measure is adopted. In order to validate the feasibility and functionality of the delay compensation measures adopted in the proposed PDC strategy, experiments were also carried out. Fig. 13(a) demonstrates the experimentally obtained waveforms without the delay compensation when the *d*-axis current is step changed. When this figure is compared with Fig. 9(a), current fluctuations can be clearly seen when the delay compensation is not used, resulting in performance deterioration of transient behaviors. Furthermore, cross-coupling effects are also introduced to the transient responses of the rectifier under this situation. It is measured from Fig. 13(a) that the current fluctuations resulting from the time

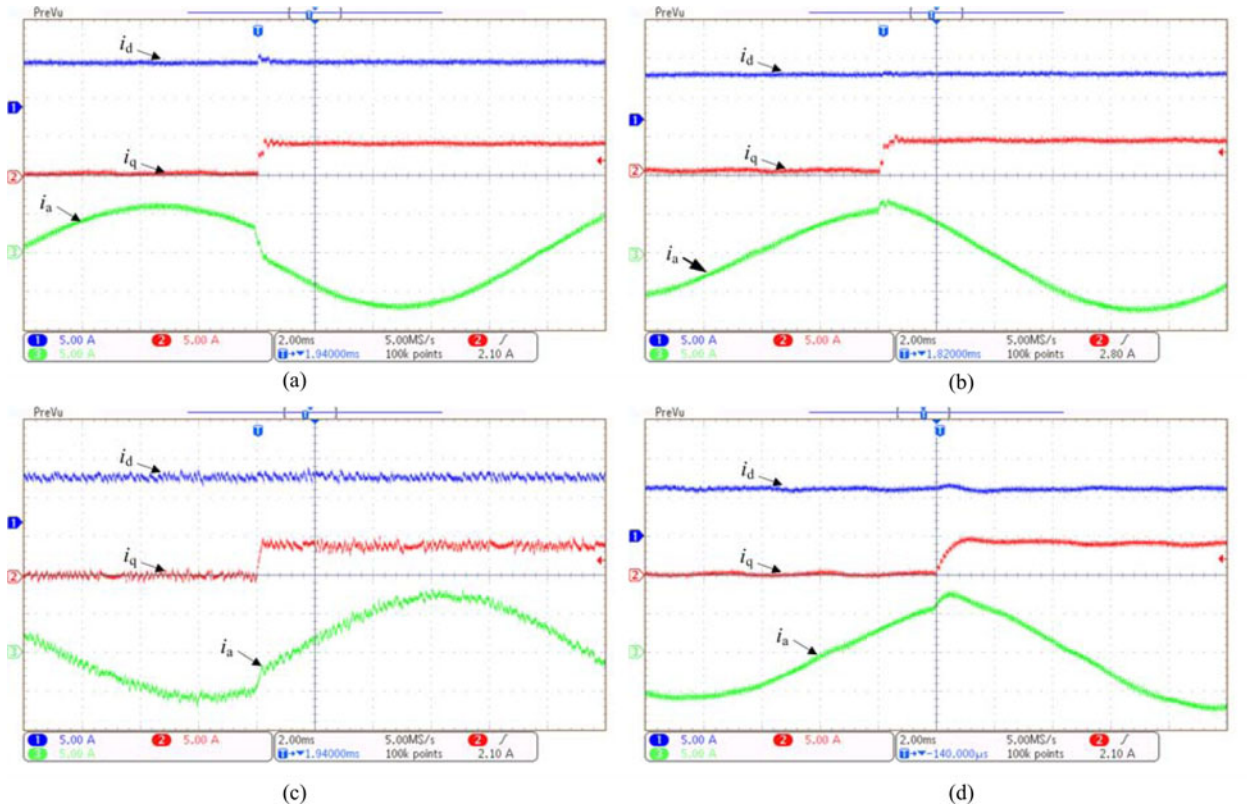

Fig. 16. Experimental results using four different control strategies during q-axis steps. (a) Conventional DBP. (b) Proposed PDC. (c) FCS-MPC. (d) Classic LC.

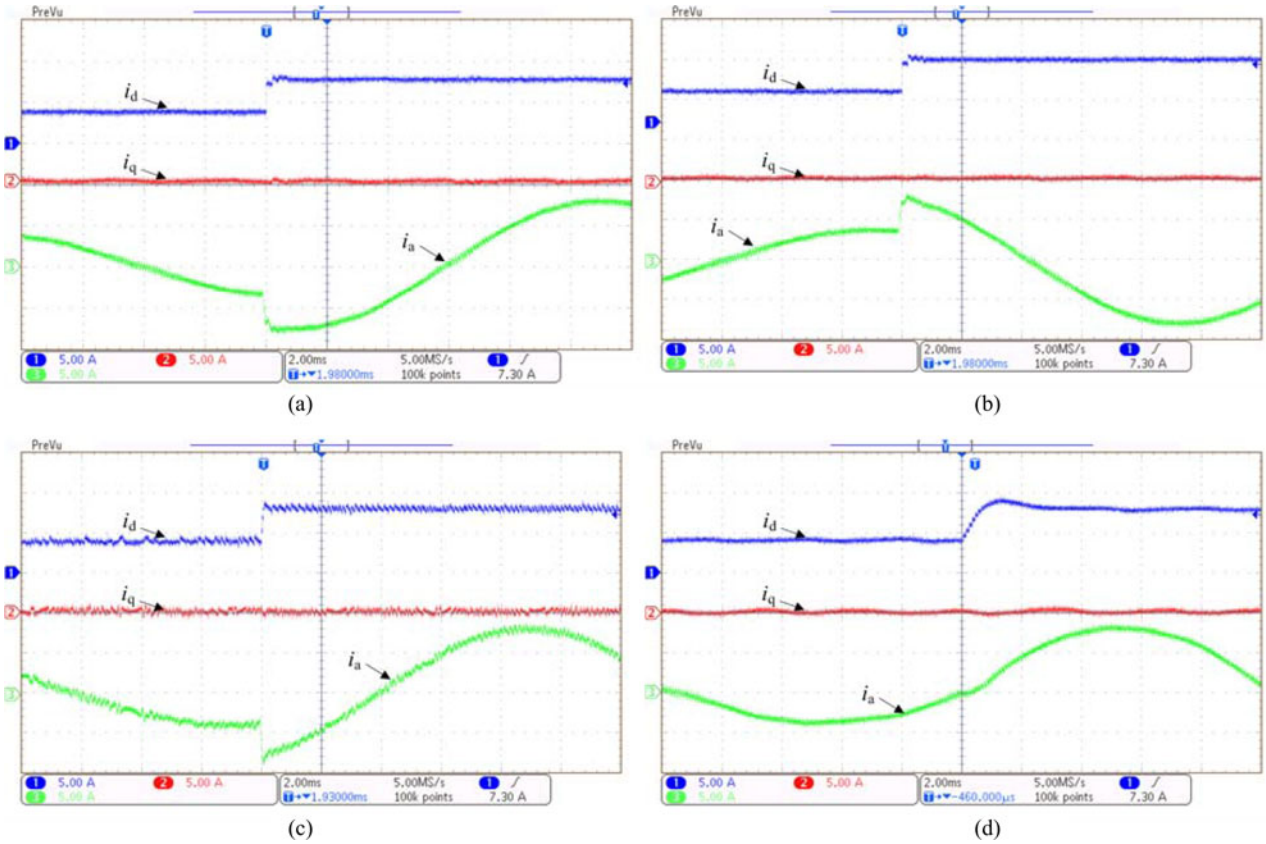

Fig. 17. Experimental results using four different control strategies during d-axis steps. (a) Conventional DBP. (b) Proposed PDC. (c) FCS-MPC. (d) Classic LC.

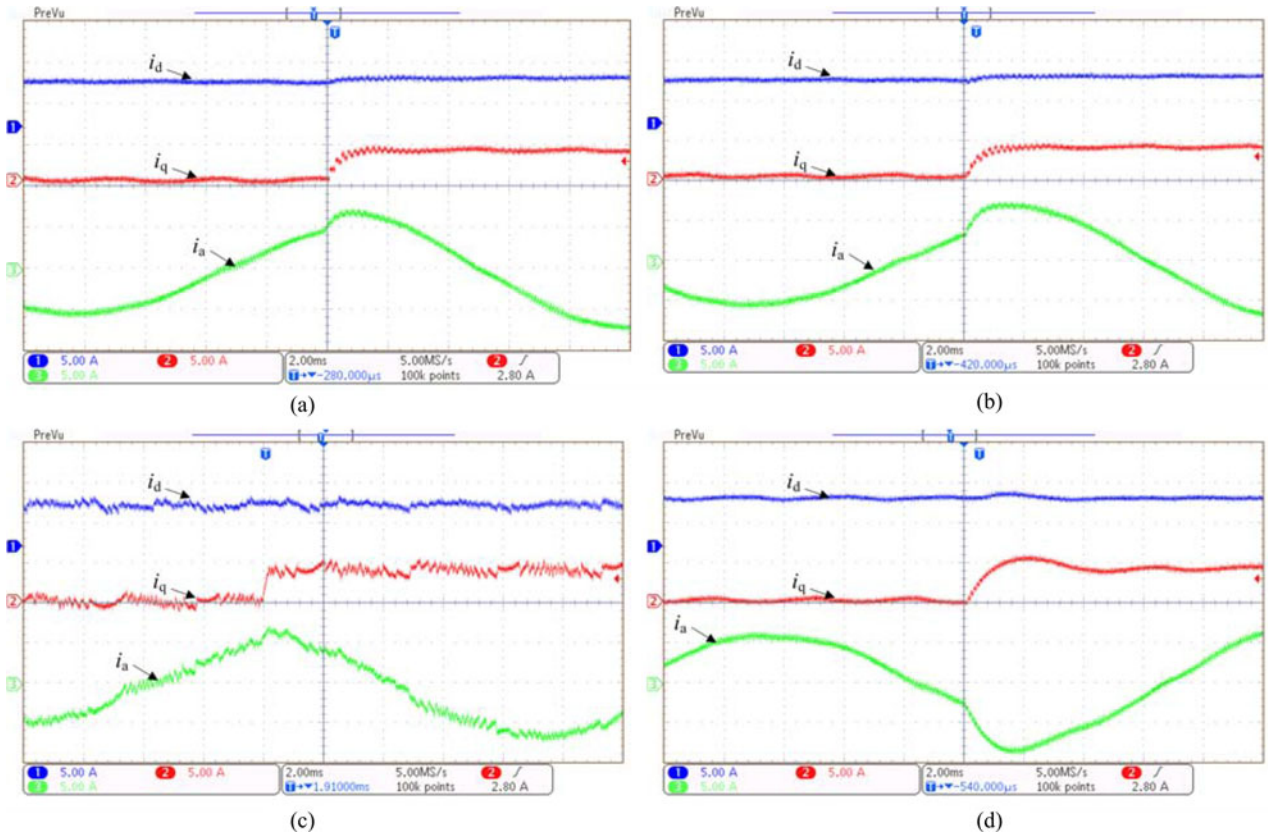

Fig. 18. Experimental results using four different control strategies with line inductance errors. (a) Conventional DBP. (b) Proposed PDC. (c) FCS-MPC. (d) Classic LC.

delay lasts around 20 ms before system behaviors return to normal. Further comparison is also shown in Figs. 9 and 13(b) with a step change of q-axis reference current. Similar conclusion can be easily obtained by comparing Figs. 13(b) and 9(b). As can be clearly observed in these illustrative waveforms, the control delay should not be neglected, especially in the case of transient processes. And the delay compensation measures mentioned previously are effective with regard to the improvement of transient responses. However, it is worth pointing out that system steady-state performances are not significantly influenced by the control delay, as shown in Fig. 13. This is due to the fact that, during steady state operation, the sampled d- and q-axes currents are both constant. The control delay could not affect these constant sampling signals.

IV. Comparison Studies

A. Comparisons of Steady-State Performances

To highlight the conceptual differences of the proposed PDC with DBP control, FCS-MPC, and classic linear control strategies (LC), in-depth comparative studies were further carried out in this section. In terms of steady-state performances, the corresponding waveforms and THD results are shown in Figs. 14 and 15. d-Axis, q-axis and phase A currents are all presented for the convenience of comparison. In general, excellent steady-state performances can be expected when PDC is adopted, whose behaviors are similar to those of DBP and LC. Zero steady-state average error and sinusoidal current waveforms can be clearly observed, as demonstrated by Fig. 14(b). Actually, this is due to the fact that the proposed PDC strategy directly determines optimal duty-cycle signals by behavior prediction and cost function minimization. Outstanding steady-state performances and optimum operations of converters within each sampling period can thus be expected. However, the steady-state performances are unsatisfactory with FCS-MPC adopted, as shown in Fig. 14(c). Even though d- and q-axes currents can both be regulated without significant steady-state errors, and the phase current is also sinusoidal, fluctuations and harmonics are clearly visible in d- and q-axes currents, as demonstrated in Figs. 14(c) and 15(c). This results in a wide trajectory band with respect to the phase currents. In addition, it is worth noting that the sampling frequency is chosen as 33 kHz during the implementation process of FCS-MPC, while the 10 kHz sampling frequency is adopted when the other three different control strategies are tested. Even though such a high sampling frequency was adopted for FCS-MPC, unsatisfactory steady-state performances were obtained. This due to the fact that, within each sampling period, FCS-MPC selects the optimal switching action based on minimization of the predefined cost function. In other words, only one voltage vector takes action within each sampling period.

It should be noted that each method has its advantages and disadvantages. Actually, the proposed PDC is an online optimizing control approach, aiming to obtain the optimal control actions under different operating conditions. Therefore, this

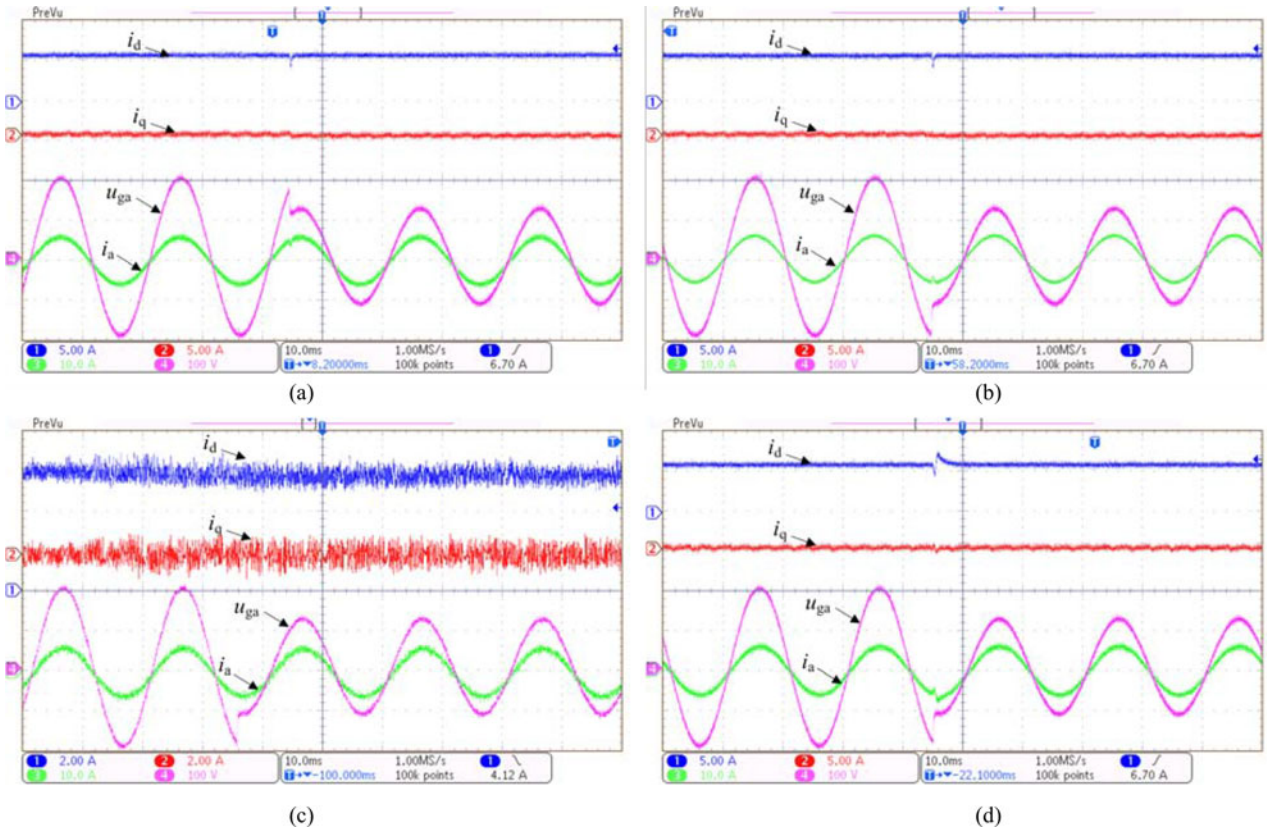

Fig. 19. Experimental results using four different control strategies during voltage dips. (a) Conventional DBP. (b) Proposed PDC. (c) FCS-MPC. (d) Classic LC.

algorithm is more complicated than traditional controllers. And its running time during implementation is a little longer than those of other control methods.

B. Comparisons of Transient Performances

On the other hand, in terms of transient responses, experiments were further conducted for comparison. As shown Fig. 16, the reference of q-axis current was step changed between 0 and 4 A with d-axis current being 6 A, while in Fig. 17 the d-axis reference current changed between 4 and 8 A with q-axis current being 0 A. As demonstrated by these experimental waveforms, fast tracking performances can be expected when DBP, the proposed PDC, and FCS-MPC are adopted, respectively, while dynamic behaviors are relatively slow when classic linear controller is used. The reason for this phenomenon is that, DBP, the proposed PDC, and FCS-MPC all belong to the family of predictive controllers, whose remarkable characteristic is the highly dynamic performance with the assistance of behavior prediction. Due to the inherent characteristics of predictive strategies, fast dynamic responses can be expected. Besides, it should be noted that, when DBP strategy is adopted, coupling phenomenon can be clearly seen under the situation of step change in current references, as demonstrated in Fig. 16(a). This is due to the fact that, when DBP strategy is used, the required output voltage of the converter is directly determined based on current errors and model information, without taking the modulation process and switching actions into account. Optimal operation of converters cannot be achieved under this situation. Nevertheless, this is not the case for the proposed PDC. With PDC adopted, d- and q-axes currents both present good dynamic responses, which is completely decoupled from each other at all times, as can be clearly visible even during dynamic transitions.

C. Comparisons of Performances Under Grid Filter Parameter Variations

For the control of three-phase active-front-end rectifiers, system robustness against model inaccuracy and parameter variations is an important aspect. In order to demonstrate the effect of errors in the model parameter values on system characteristics, relative experiments using four different control strategies mentioned earlier were also conducted. Fig. 18 shows system behaviors with the inductance value adopted in the control strategy changed by 60%. During the testing process, the q-axis reference current is step-up changed from 0 to 4 A, with the d-axis current demand remaining 6 A. When the experimental results shown in Fig. 18 are compared with those shown in Fig. 16, where no inductance error was introduced, it is clearly visible that disturbances resulting from parametric variations bring influences on system behaviors when DBP, the proposed PDC, and FCS-MPC are adopted, respectively. This is due to the fact that all these three control strategies belong to the family of predictive controllers, whose inherited

characteristic is system performance prediction based on converter model information.

D. Comparisons of Performances Under External Disturbances

With the aim of evaluating system performances under the situation of external disturbances, Fig. 19 demonstrates experimental results using four different control strategies when voltage dips were introduced to the ac supply grid. These results were obtained under the operating conditions with *d*- and *q*-axes reference current being 6 and 0 A, respectively. Due to the high bandwidth possessed by predictive controllers including DBP, PDC, and FCS-MPC, *d*- and *q*-axes currents can both be properly regulated immediately after the dip moment. Highly dynamic transient behaviors can be successfully achieved. However, this is not the case for classic linear controllers. Because of its relative slow responses, significant current fluctuations can be observed at the instant of voltage dip.

V. Conclusion

With the aim of proposing one type of online optimizing control for three-phase active-front-end rectifiers, this paper presents a PDC control strategy. The effects of duty cycles on instantaneous current variations are first predicted. As an important factor for the solving process of the optimizing problem, a cost function is previously constructed based on the desired control performance. The optimal duty cycles are determined by minimizing the cost function. Therefore, the application of optimal duty cycles automatically ensures optimum operations of converters within each sampling period. Different from classic linear controllers, the proposed PDC belongs to the family of predictive controllers. Highly dynamic responses can thus be expected with PDC adopted. Besides, when PDC is compared with traditional DBP, its superiority lies in its online optimization characteristics based on cost function minimization, which has been confirmed by experimental results. Furthermore, even though FCS-MPC is also one type of online optimization algorithm, the optimal voltage vector that minimizes the cost function is selected and applied, leading to varying switching frequency and deteriorations in steady-state performances. Differently, the optimal duty cycles are determined with respect to the proposed PDC; distinguished performances can thus be expected.

References

[1] P. Cortés, M. P. Kazmierkowski, R. M. Kennel, D. E. Quevedo, and J. Rodriguez, "Predictive control in power electronics and drives," *IEEE Trans. Ind. Electron.*, vol. 55, no. 2, pp. 4312–4324, Dec. 2008.

[2] Z. Song, C. Xia, and T. Liu, "Predictive current control of three-phase grid-connected converters with constant switching frequency for wind energy systems," *IEEE Trans. Ind. Electron.*, vol. 60, no. 6, pp. 2451–2464, Jun. 2013.

[3] Z. Song, W. Chen, and C. Xia, "Predictive direct power control for three-phase grid-connected converters without sector information and voltage vector selection," *IEEE Trans. Power Electron.*, vol. 29, no. 10, pp. 5518–5531, Oct. 2014.

[4] F. Blaabjerg, R. Teodorescu, M. Liserre, and A. V. Timbus, "Overview of control and grid synchronization for distributed power generation systems," *IEEE Trans. Ind. Electron.*, vol. 53, no. 5, pp. 1398–1409, Oct. 2006.

[5] S. Buso, L. Malesani, and P. Mattavelli, "Comparison of current control techniques for active filter applications," *IEEE Trans. Ind. Electron.*, vol. 45, no. 5, pp. 722–729, Oct. 1998.

[6] A. Timbus, M. Liserre, R. Teodorescu, P. Rodriguez, and F. Blaabjerg, "Evaluation of current controllers for distributed power generation systems," *IEEE Trans. Power Electron.*, vol. 24, no. 3, pp. 654–664, Mar. 2009.

[7] J. Rodriguez, M. P. Kazmierkowski, J. R. Espinoza, P. Zanchetta, H. Abu-Rub, H. A. Young, and C. A. Rojas, "State of the art of finite control set model predictive control in power electronics," *IEEE Trans. Ind. Informat.*, vol. 9, no. 2, pp. 1003–1016, May 2013.

[8] R. P. Aguilera, P. Lezana, and D. E. Quevedo, "Finite-control-set model predictive control with improved steady-state performance," *IEEE Trans. Ind. Electron.*, vol. 9, no. 2, pp. 658–667, May 2013.

[9] M. Rivera, V. Yaramasu, A. Llor, J. Rodriguez, B. Wu, and M. Fadel, "Digital predictive current control of a three-phase four-leg inverter," *IEEE Trans. Ind. Electron*., vol. 60, no. 11, pp. 4903–4912, Nov. 2013.

[10] M. A. Perez, J. Rodriguez, E. J. Fuentes, and F. Kammerer, "Predictive control of AC–AC modular multilevel converters," *IEEE Trans. Ind. Electron.*, vol. 59, no. 7, pp. 2832–2839, Jul. 2012.

[11] V. Yaramasu and B. Wu, "Model predictive decoupled active and reactive power control for high-power grid-connected four-level diode-clamped inverters," *IEEE Trans. Ind. Electron.*, vol. 61, no. 7, pp. 3407–3416, Jul. 2014.

[12] H. Guzman, M. J. Duran, F. Barrero, B. Bogado, and S. Toral, "Speed control of five-phase induction motors with integrated open-phase fault operation using model-based predictive current control techniques," *IEEE Trans. Ind. Electron.*, vol. 61, no. 9, pp. 4474–4475, Sep. 2014.

[13] B. S. Riar, T. Geyer, and U. K. Madawala, "Model predictive direct current control of modular multilevel converters: Modelling, analysis and experimental evaluation," *IEEE Trans. Power Electron.*, vol. 30, no. 1, pp. 431–439, Jan. 2015.

[14] M. Preindl, E. Schaltz, and P. Thøgersen, "Switching frequency reduction using model predictive direct current control for high-power voltage source inverters," *IEEE Trans. Ind. Electron.*, vol. 58, no. 7, pp. 2826–2835, Jul. 2011.

[15] Y. Zhang and W. Xie, "Low complexity model predictive control—Single vector based approach," *IEEE Trans. Power Electron.*, vol. 29, no. 10, pp. 5532–5541, Oct. 2014.

[16] T. Geyer and D. E. Quevedo, "Multistep finite control set model predictive control for power electronics—Part 1: Algorithm," *IEEE Trans. Power Electron.*, vol. 29, no. 12, pp. 6836–6846, Dec. 2014.

[17] C. S. Lim, N. A. Rahim, W. P. Hew, and E. Levi, "Model predictive control of a two-motor drive with five-leg-inverter supply," *IEEE Trans. Ind. Electron*., vol. 60, no. 1, pp. 54–65, Jan. 2013.

[18] C. A. Rojas, J. Rodríguez, F. Villarroel, J. R. Espinoza, C. A. Silva, and M. Trincado, "Predictive torque and flux control without weighting factors," *IEEE Trans. Ind. Electron*., vol. 60, no. 2, pp. 681–690, Feb. 2013.

[19] F. Villarroel, J. R. Espinoza, C. A. Rojas, J. Rodriguez, M. Rivera, and D. Sbarbaro, " Multiobjective switching state selector for finite-states model predictive control based on fuzzy decision making in a matrix converter," *IEEE Trans. Ind. Electron.*, vol. 60, no. 2, pp. 589–599, Feb. 2013.

[20] V. Yaramasu, M. Rivera, M. Narimani, B. Wu, and J. Rodriguez, "Model predictive approach for a simple and effective load voltage control of four-leg inverter with an output LC filter," *IEEE Trans. Ind. Electron.*, vol. 61, no. 10, pp. 5259–5270, Oct. 2014.

[21] C. Lin, T. Liu, J. Yu, L. C. Fu, and C. F. Hsiao, "Model-free predictive current control for interior permanent-magnet synchronous motor drives based on current difference detection technique," *IEEE Trans. Ind. Electron.*, vol. 61, no. 2, pp. 667–681, Feb. 2014.

[22] S. Kwak, U. Moon, and J. Park, "Predictive-control-based direct power control with an adaptive parameter identification technique for improved AFE performance," *IEEE Trans. Power Electron.*, vol. 29, no. 11, pp. 6178–6187, Nov. 2014.

[23] Y. Zhang, W. Xie, Z. Li, and Y. Zhang, "Low complexity model predictive power control: Double vector based approach," *IEEE Trans. Ind. Electron.*, vol. 61, no. 11, pp. 5871–5880, Nov. 2014.

[24] Y. Zhang and H. Yang, "Model predictive torque control of induction motor drives with optimal duty cycle control," *IEEE Trans. Power Electron.*, vol. 29, no. 12, pp. 6593–6603, Dec. 2014.

[25] Y. Zhang, W. Xie, Z. Li, and Y. Zhang, "Model predictive direct power control of a PWM rectifier with duty cycle optimization," *IEEE Trans. Power Electron.*, vol. 28, no. 11, pp. 5343–5351, Nov. 2013.

[26] P. E. Kakosimos, A. G. Kladas, and S. N. Manias, "Fast photovoltaic-system voltage-or current-oriented MPPT employing a predictive digital current-controlled converter," *IEEE Trans. Ind. Electron.*, vol. 60, no. 12, pp. 5673–5685, Dec. 2013.
[27] S. Kouro, P. Corés, R. Vargas, U. Ammann, and J. Rodríguez, "Model predictive control—A simple and powerful method to control power converters," *IEEE Trans. Ind. Electron.*, vol. 56, no. 6, pp. 1826–1838, Jun. 2009.
[28] P. Corés, J. Rodríguez, D. E. Quevedo, and C. Silva, "Predictive current control strategy with imposed load current spectrum," *IEEE Trans. Power Electron.*, vol. 23, no. 2, pp. 612–618, Mar. 2008.
[29] J. Hu, J. Zhu, Y. Zhang, G. Platt, Q. Ma, D. G. Dorrell, "Predictive direct virtual torque and power control of doubly fed induction generators for fast and smooth grid synchronization and flexible power regulation," *IEEE Trans. Power Electron.*, vol. 28, no. 7, pp. 3182–3194, Jul. 2013.

Zhanfeng Song (M'13) was born in Hebei, China, in 1982. He received the B.S., M.S., and Ph.D. degrees from Tianjin University, Tianjin, China, in 2004, 2006, and 2009, respectively, all in electrical engineering.

He is currently an Associate Professor in the School of Electrical Engineering and Automation, Tianjin University. His research interests include electrical machines and their control systems.

Yanjun Tian (S'14) received the B.Sc. and M.Sc. degrees in electrical engineering from the Yanshan University, Qinhuangdao, China, in 2009 and 2012, respectively, and is currently working toward the Ph.D. degree in the Department of Energy Technology, Aalborg University, Aalborg, Denmark.

His research interest includes distributed generation and active distribution network control, focusing on the impedance interaction, cascaded converter control, and the parallel connected converter control.

Wei Chen (M'12) was born in Shanxi, China, in 1977. He received the B.Sc., M.Sc., and Ph.D. degrees in electrical engineering from Tianjin University, Tianjin, China, in 2000, 2003, and 2006, respectively.

In 2006, he joined Tianjin University as a Lecturer. Since 2009, he has been an Associate Professor in the School of Electrical Engineering and Automation. His research interests include modeling optimization of electrical machines and their drivers.

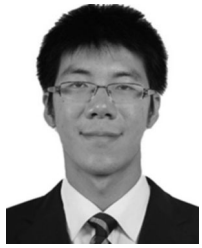

Zhibin Zou was born in Jiangxi, China, in 1983. He received the B.S. and M.S. degrees from Tianjin University, Tianjin, China, in 2004 and 2007, respectively, both in electrical engineering.

He is currently an Engineer with the State Grid Jiangxi Electric Power Company, Nanchang, China. His research interests include electrical machines and their control systems.

Zhe Chen (M'95–SM'98) received the B.Eng. and M.Sc. degrees from the Northeast China Institute of Electric Power Engineering, Jilin City, China, and the Ph.D. degree from the University of Durham, Durham, U.K.

He is a Full Professor in the Department of Energy Technology, Aalborg University, Aalborg, Denmark. He is the Leader of Wind Power System Research program at the Department of Energy Technology, Aalborg University and the Danish Principle Investigator for Wind Energy of Sino-Danish Centre for Education and Research. His research areas are power systems, power electronics and electric machines; his main current research interests are wind energy and modern power systems. He has led many research projects and has more than 400 publications in his technical field.

Dr. Chen is an Editor of the IEEE TRANSACTIONS ON POWER SYSTEMS, an Associate Editor of the IEEE TRANSACTIONS ON POWER ELECTRONICS, a Fellow of the Institution of Engineering and Technology (London, U.K.), and a Chartered Engineer in the U.K.